Received: 29 March 2017 | Accepted: 15 July 2017

DOI: 10.1111/jace.15100

ORIGINAL ARTICLE

Journal of the American Ceramic Society

Comparative study of Al_2O_3, HfO_2, and $HfAlO_x$ for improved self-compliance bipolar resistive switching

Andrey S. Sokolov | Seok Ki Son | Donghwan Lim | Hoon Hee Han | Yu-Rim Jeon | Jae Ho Lee | Changhwan Choi

Division of Materials Science and Engineering, Hanyang University, Seoul, Korea

Correspondence
Changhwan Choi, Division of Materials Science and Engineering, Hanyang University, Seoul, Korea.
Email: cchoi@hanyang.ac.kr

Funding information
Ministry of Education, Science and Technology, Grant/Award Number: NRF-2015R1D1A1A01060300

Abstract

The comparison of resistive switching (RS) storage in the same device architecture is explored for atomic layer deposition (ALD) Al_2O_3, HfO_2 and $HfAlO_x$-based resistive random access memory (ReRAM) devices. Among them, the deeper high- and low- resistance states, more uniform V_{SET}-V_{RES}, persistent R_{OFF}/R_{ON} ($>10^2$) ratio and endurance up to 10^5 cycles during both DC and AC measurements were observed for $HfAlO_x$-based device. This improved behavior is attributed to the intermixing of amorphous Al_2O_3/HfO_2 oxide layers to form amorphous thermally stable $HfAlO_x$ thin films by consecutive-cycled ALD. In addition, the higher oxygen content at Ti/$HfAlO_x$ thin films interface was found within the energy dispersive spectroscopy analysis (EDS). We believe this higher oxygen content at the interface could lead to its sufficient storage and supply, leading to the stable filament reduction-oxidation operation. Further given insight to the RS mechanism, SET/RESET power necessities and scavenging effect shed a light to the enhancement of $HfAlO_x$-based ReRAM device as well.

KEYWORDS
dielectric materials/properties, electrical properties, semiconductors, thin

1 | INTRODUCTION

Among the promising nonvolatile memory candidates to replace the FLASH memory for the big data storage, the resistive random access memory (ReRAM) appears to be the most suitable alternative due to its scaling, power and speed characteristics.[1,2] Extensive research has been done among various storage transition metal oxides and many of them such as NiO[3], TiO_2[4], ZrO_2[5], Ta_2O_5[6,7], HfO_2[8-10] and others[11,12] can be utilized in a new ReRAM technology. Among all, lots of attention has been put these days to the HfO_2 ReRAM due to its stable high endurable resistive switching (RS) behavior and compatibility within the complementary metal oxide semiconductor (CMOS) technology process.[13]

However, the commercialization of such HfO_2 ReRAM devices is yet to be achieved due to the variability and nonuniform RS behavior, resulting from stochastic nature of the conductive filament path formation and impact of different oxygen vacancies profiles.[14,15] It has been reported that the conductive filaments can form along the grain boundaries of the switching material especially in HfO_x-based ReRAM.[16] Therefore, the variability and switching properties can be significantly influenced by the crystallinity of the switching material. To say more, polycrystalline HfO_2 films are not desirable to perform RS behavior due to strong dependence HfO_2 thin film morphology on the Ti/HfO_2 interface reactivity.[17] The low crystallization temperature (<400°C) of HfO_2 thin films is crucial issue during the ReRAM operation process due to the oxygen deficiency filament paths formation along the grain boundaries causing the big variation in the RS performance.[18,19] One of the possible ways to keep HfO_2 thin films amorphous is to introduce Al-doping into HfO_2 oxide by atomic layer deposition

(ALD) to improve its thermal stability (>900°C).[20] However, few systematic results on $HfAlO_x$-based ReRAM and its comparison with other dielectrics are reported so far.

We found that layer by layer intermixing of the amorphous Al_2O_3 with the HfO_2 thin films during ALD super cycling leads to superior RS characteristics compared to only binary Al_2O_3 and HfO_2-based ReRAM devices. In this letter, we have investigated RS characteristics of Al_2O_3, HfO_2 and $HfAlO_x$-based ReRAM devices with the same device structure. All the devices were confirmed to have amorphous phase and same oxide thicknesses by X-ray diffractometer (XRD) analysis and transmission electron microscopy (TEM) as well as ellipsometry, respectively. The RS properties of each device were examined by continuous DC sweep up to 400 cycles. Among these devices, the $HfAlO_x$-based ReRAM devices showed improved high- and low- resistance states (HRS & LRS) as long as more uniform V_{SET}-V_{RES} distributions, while maintaining sustainable R_{OFF}/R_{ON} (>10^2) ratio. Such an improvement leads to the desirable low power consumption and low operation current device. In addition, switching mechanism, endurance and retention characteristics are also discussed.

2 | EXPERIMENTAL PROCEDURE

All devices were prepared on the Si/SiO_2 substrates. These substrates were cleaned with standard cleaning procedure including dip in acetone (99.9%) and methanol (99.9%) in a sequence followed by rinsing with de-ionized water and drying by N_2 blow. Then, Ti of 5 nm and Pt of 50 nm thicknesses were deposited as bottom electrodes (BE) by DC and reactive sputtering at the chamber pressure of 6.1×10^{-6} and 1.5×10^{-2} Torr, respectively. Immediately after, the insulating films of approximately 6.5 nm thickness of Al_2O_3, HfO_2, and $HfAlO_x$ were prepared under the same ALD conditions at 250°C using trimethyl-aluminum (TMA) and tetraethyl-methyl-amino-Hf (TEMA-Hf) precursors, respectively, with H_2O as an oxidant. Particularly, nano-laminated $HfAlO_x$ films with the 1:1 ratio of Hf and Al were obtained by super ALD cycling of Al_2O_3 and HfO_2 oxides. The deposition rates for Al_2O_3 and HfO_2 oxides were 1.3 and 0.85 Å/cycle, respectively. Finally, top electrode (TE) of 50 nm thick Ti were deposited by DC magnetron sputtering and patterned using conventional photolithography technique to the square patterns of 100×100 μm^2. The schematic cross-section of all devices is shown in Figure 1A. The crystal structure of the HfO_2 and $HfAlO_x$ thin films was examined by X-ray diffraction (HR-XRD, Rigaku SmartLab, CuK_α radiation) analysis. By Transmission electron microscopy (TEM, JEM-2100F), the physical thickness, cross-sectional morphology and energy dispersive spectroscopy were defined and carried out. The current–voltage (*I–V*) characteristics were performed on the Keithley 4200-SCS semiconductor characterization system at the room temperature and atmospheric pressure. Bias was applied on Ti top electrode (TE) while Pt bottom electrode (BE) was grounded.

3 | RESULTS AND DISCUSSION

Figure 1B,C show the TEM images and EDS analysis of the devices with Al_2O_3, HfO_2, and $HfAlO_x$ oxides sandwiched between Ti (TE) and Pt (BE) to confirm the layer thicknesses and extract atomic composition of elements, respectively. All samples show similar physical oxide thicknesses within ~6.5 nm. The bold yellow line represents the direction of EDS analysis. Figure 1C shows the EDS analysis in which the clear difference of oxygen (O^{-2}) amount at the Ti/oxide interface can be seen in the red boxes for each device and the corresponding atomic percentage of existing elements for each device is summarized in the Table 1 as well. We believe this difference of oxygen (O^{-2}) species at the Ti/oxide interface is one of the significant causes affecting resistive switching (RS) behavior of Al_2O_3, HfO_2 and $HfAlO_x$-based devices as we demonstrate later.

The XRD analysis of HfO_2 and $HfAlO_x$ thin films revealed that although the ALD deposition temperature was quite low 250°C, the clear difference in amorphous phase can be seen in Figure 2. No peak, except HfO_2 (002), can be distinguishable. However, in the angle range 2θ (26°-36°) different XRD behavior is observed for HfO_2 films similar to the reported results of monoclinic phase with lattice (111) and (−111) appeared at higher temperatures.[17] In case of HfO_2 thin film, the only single broad peak is found which indicates the formation of amorphous phase containing the few nanometer crystallites of monoclinic phase so far. Extensive studies on formation of conductive filament along grain boundaries (GBs) in HfO_2-based RRAM has been done.[21-23] Particularly, GBs in monoclinic phase of HfO_2 oxide serves as deca-nanometre paths for oxygen vacancies segregation, which are conductive, and the size and number of such paths is strongly dependent on electroforming breakdown (BD) hardness (high electric field applied >10 MV/cm). Due to this filament size control through the GBs seems impractical. In addition, Lanza et al. showed results on probing HfO_2 thin films with conductive atomic force microscope (CAFM) and discovered that current leaky sites are much smaller in case of amorphous HfO_2 dielectrics.[23] Later, Calka et al. showed that HfO_2 thin films with GBs are lack of oxygen scavenging ability at Ti/HfO_2 interface, which is required prior stable

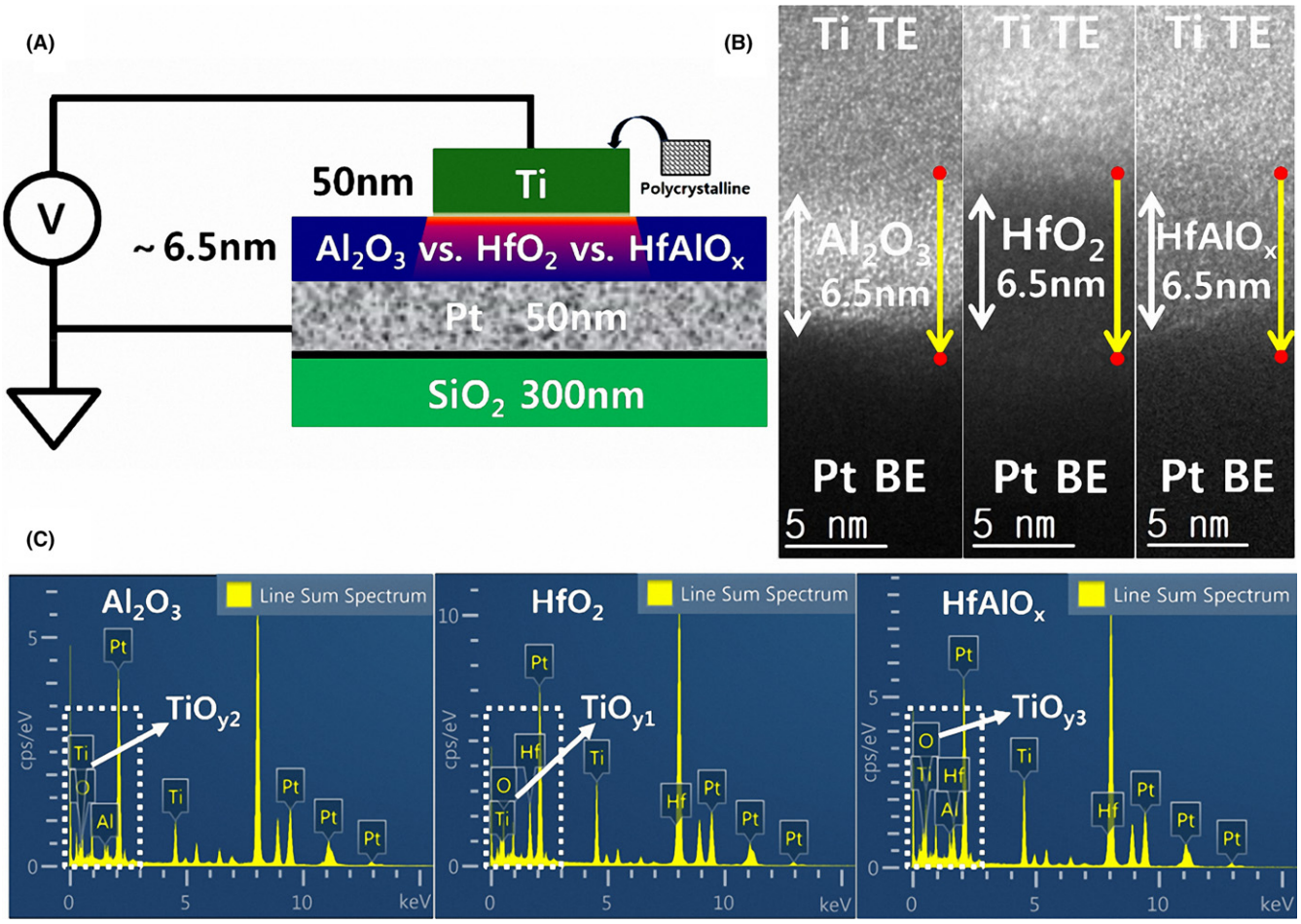

FIGURE 1 (A) A schematic cross-section diagram of the device, (B) TEM images of Al_2O_3, HfO_2 and $HfAlO_x$-based ReRAM devices, and (C) EDS atomic element analysis of each device, where white box shows the oxygen and titanium elements difference at the Ti/oxide interface from device-to-device [Color figure can be viewed at wileyonlinelibrary.com]

TABLE 1 Atomic percentage (%) of elements within Al_2O_3, HfO_2 and $HfAlO_x$-based ReRAM devices

Device structure	O	Ti	Pt	Al	Hf
$Ti/Al_2O_3/Pt$	25.64	21.91	44.81	7.64	–
$Ti/HfO_2/Pt$	33.89	29.36	29.70	–	7.05
$Ti/HfAlO_x/Pt$	36.91	24.57	24.85	7.85	5.82

RS device operation.[17] Here, we imply that nanocrystalline phase in HfO_2 thin films could result in big size of filament formation by providing additional/uncontrollable oxygen vacancies paths at nanocrystalline defect sites. Therefore, amorphizer such an Al_2O_3 alloyed into HfO_2 thin film matrix is necessary and $HfAlO_x$ thin films appeared with its more amorphous phase result as shown in Figure 2, which indicates its higher amorphous thermal stability and further, contribution to thinner high resistive filament formation.

Figure 3 shows the forming voltage (V_{form}) of each Al_2O_3, HfO_2 and $HfAlO_x$-based ReRAM device and its distribution from device-to-device. The thin gray lines correspond to device-to-device variation and bold lines are average of V_{form} curves as shown in Figure 3A. Recently, it has been proved that the current compliance and stress mode during the V_{form} process affects geometrical and physical characteristics of the filament significantly.[24] To consider this we performed V_{form} under the same current compliance (~1 μA) for HfO_2 and $HfAlO_x$-based devices and (~10 μA) for Al_2O_3-based as shown in Figure 3A. The minimum current compliance value was assessed for each device after which the robust RS behavior obtained. The highest average forming voltage (V_{form}=3.85 V) is observed for Al_2O_3-based device, whereas for HfO_2 and $HfAlO_x$-based one the average V_{form} values are 3.45 V and 3.75 V, respectively. Further, soft breakdown for Al_2O_3-based device occurs under higher current compliance (I_{CC}=10 μA) compared to HfO_2 and $HfAlO_x$-based one (I_{CC}=1 μA). This can be attributed to the naturally large band gap of Al_2O_3 thin films and its higher strength to breakdown. Although, in case of Al_2O_3 and $HfAlO_x$-based devices the V_{form} is a bit higher than that for HfO_2-based

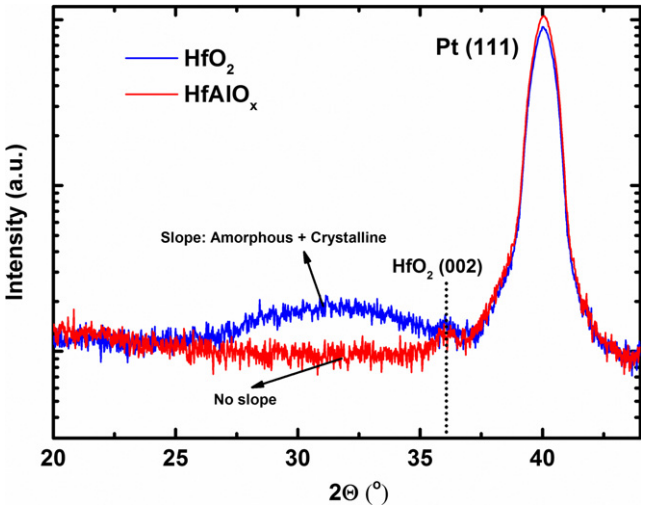

FIGURE 2 XRD patterns of as-deposited HfO_2 and $HfAlO_x$ thin films on Pt/SiO_2 substrates prepared by ALD 250°C [Color figure can be viewed at wileyonlinelibrary.com]

one, the more uniform forming voltage V_{form} from device-to-device is clearly observed for both of the devices. Moreover, the V_{form} of dielectric materials is strongly dependent on the dielectric constant (k) as $1/\sqrt{k}$.[25] The standard dielectric constant values of Al_2O_3 and HfO_2 oxides are ~9 and ~23, respectively. And in case of $HfAlO_x$ nanolaminate thin films within the composition ratio of 1:1 (Hf:Al), the dielectric constant constitutes ~17.[26,27] Apparently, increase in Al% composition in the HfO_2 thin films results in gradual decrease in dielectric constant. Due to this, an intermediate forming voltage (V_{form}=3.75 V) in between of Al_2O_3 and HfO_2-based devices is observed in case of $HfAlO_x$-based device. In Figure 3B the device-to-device distribution is observed for each device type. None of them show uniform distribution due to the forming voltage V_{form} tails presence. However, lower V_{form} can be noticed for HfO_2-based device, while higher and intermediate V_{form} values are observed for Al_2O_3 and $HfAlO_x$-based devices, respectively.

Typical I–V switching curves of each Al_2O_3, HfO_2 and $HfAlO_x$-based ReRAM devices within the first 100 and last 400 RS cycles are shown in Figure 4A,B, respectively. All devices show repeatable self-compliance switching behavior more than one order of magnitude (>10×) during the first 100 cycles. However, during the last 400 cycles, the severe degradation of the high resistant state (HRS) was observed for Al_2O_3-based device whereas the HRS of HfO_2 and $HfAlO_x$-based one changes insignificantly. To say more, the $HfAlO_x$-based device shows clear higher resistance in the low resistance state (LRS), compared to other devices and can be programmed at lower read/write current. In addition, the resistance in HRS of $HfAlO_x$-based device is found to be higher than for other devices as well, resulting with no change in effective switching R_{OFF}/R_{ON} window from other devices and it can be seen in Figure 6A. We believe that nanolaminated nature of the $HfAlO_x$ thin films is responsible for that, i.e. incorporation of multiple Al_2O_3 layers into HfO_2 films can confine the RS filament shape and result in current lowering during the SET-RESET switching process. In addition, higher oxygen O^{-2} content at the Ti/oxide interface can also result in resistance lowering of LRS.[28,29] In Figure 1C, the EDS analysis and Table 1 support the higher oxygen O^{-2} content at the Ti/oxide interface to be in case of $HfAlO_x$ thin films compared to others. It is known that competitive bonds appear in $HfAlO_x$ thin films due to Al–O (1.93 Å) and Hf–O (2.16 Å) bond length difference and due to that thin film becomes denser than binary HfO_2 thin film. Therefore, we

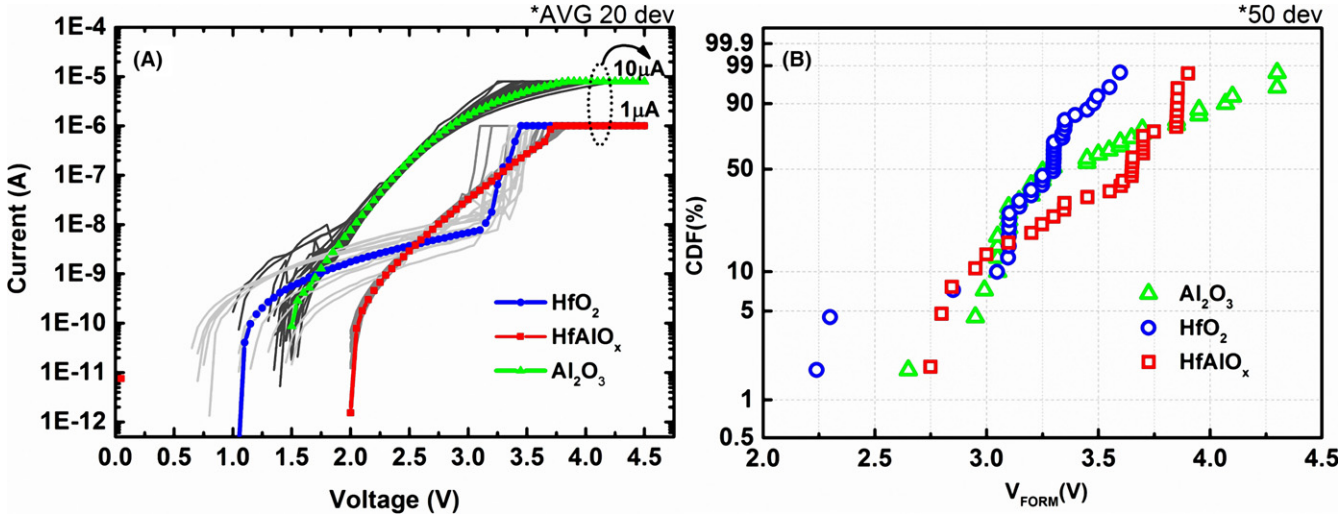

FIGURE 3 (A) Forming voltage for each device under the current compliance limitation, (B) CDF of forming voltages V_{form} for each Al_2O_3, HfO_2 and $HfAlO_x$-based devices [Color figure can be viewed at wileyonlinelibrary.com]

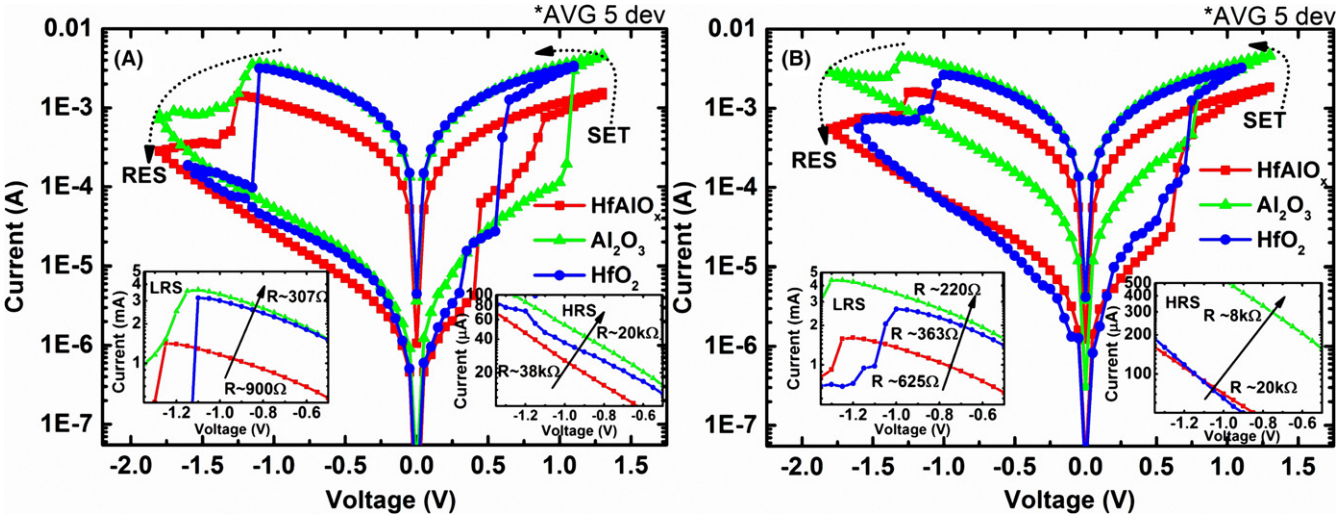

FIGURE 4 (A) Typical *I–V* self-compliance switching characteristics of Al_2O_3, HfO_2 and $HfAlO_x$-based devices in the beginning 100th switching cycles, (B) at the end 400th switching cycles. The insets show average high and low resistance states (HRS & LRS) for each device [Color figure can be viewed at wileyonlinelibrary.com]

believe that reactive titanium (Ti) electrode could help to scavenge more oxygen from the $HfAlO_x$ thin films due to released internal stress and favorable atomic reconfiguration of the $HfAlO_x$ thin films. The average values of LRS are $R_{LRS}\approx900\ \Omega$ for $HfAlO_x$-based device and $R_{LRS}\approx307\ \Omega$ for Al_2O_3 and HfO_2-based one. Both the HRS & LRS of all devices deviate from its original average value in comparison within the first and last RS processes as can be seen in insets of Figure 4A,B.

Figure 5 shows schematic explanation of two particular mechanisms occurring during the RS behavior for the above phenomena of HRS degradation for Al_2O_3-based device and improvement of LRS for $HfAlO_x$-based one: (1) the top electrode (TE) Ti reactive metal scavenging effect and (2) oxygen-ions drift model. The scavenging effect is attributed to the reactive Ti metal ability to extract oxygen O^{-2} from the oxide thin film at the Ti/oxide interface and form thin TiO_y layer. Due to this oxygen O^{-2} extraction, the thin oxide film becomes sub-stoichiometric and oxygen vacancies (V_o^{2+}) are introduced inside the thin oxide film. The ability of oxygen O^{-2} extraction is measured by Gibbs free energy of oxide formation and for Ti this value is -940 kJ/mol at the room temperature.[30] Considering the values of Gibbs free energy oxide formation of Al_2O_3 and HfO_2 oxides which are -1500 kJ/mol and -1000 kJ/mol, respectively, we can conclude that scavenging effect is more favorable at Ti/HfO_2 interface than at Ti/Al_2O_3 and under applied bias this difference affects RS behavior significantly. To summarize above, chemical equation is implied to describe thermodynamic ensemble, including Ti deposition on different oxides and accounted as reaction occurring at the Ti/oxide interface:

$$\mathrm{Ti(bulk)} + \left\{\begin{array}{l}\mathrm{HfO_2}\\ \mathrm{Al_2O_3}\\ \mathrm{Hf_{1-x}Al_{2x}O_{2+x}}\end{array}\right\} \rightarrow \mathrm{TiO_{y1,y2,y3}} + \left\{\begin{array}{l}\mathrm{HfO_{2-y1}}\\ \mathrm{Al_2O_{3-y2}}\\ \mathrm{Hf_{1-x}Al_{2x}O_{(2+x)-y3}}\end{array}\right\} \quad (1)$$

where $y1>y3>y2$, and $x=0.5$, corresponding to the proportion of Al_2O_3 deposition in ALD, to reflect the correct Hf/Al ratio (1:1) respecting $Hf_{1-x}Al_{2x}O_{2+x}$ stoichiometry. The contact of reactive Ti (TE) metal with the thin oxide films results in different sub-stoichiometry of these films due to the difference in values of Gibbs free energy oxide formation. Moreover, due to Ti scavenging ability, the formation of oxygen vacancies at the Ti/oxide interface is expected, therefore, according to Kröger–Vink notation:[31]

$$\mathrm{O_o^x} \leftrightarrow \mathrm{V_o^{\bullet\bullet}} + 2\mathrm{e'} + \frac{1}{2}\mathrm{O_2(g)} \quad (2)$$

where $\mathrm{O_o^x}, \mathrm{V_o^{\bullet\bullet}}$, and $\mathrm{e'}$ are neutral oxygen ion, doubly charged oxygen vacancy and electron, respectively. The formation of TiO_y oxide with various point defects such as oxygen vacancies, interstitial or substitutional Ti^{3+} ions, and interstitial Ti^{4+} ions is also expected and noted as,

$$2\mathrm{Ti_{Ti}^x} + \mathrm{O_o^x} \leftrightarrow \frac{1}{2}\mathrm{O_2(g)} + 2\mathrm{Ti_{Ti}'} + \mathrm{V_o^{\bullet\bullet}} \quad (3)$$

where $\mathrm{Ti_{Ti}^x}$, and $\mathrm{Ti_{Ti}'}$ are normal Ti^{4+} ion at Ti^{4+} site with zero effective charge, and substitutional Ti^{3+} at Ti^{4+} site with one positive charge, respectively. Importantly, in case of $HfAlO_x$, doping Al_2O_3 oxide into HfO_2 matrix can

generate additional oxygen vacancies, according to the notation:

$$Al_2O_3 \xrightarrow{2HfO_2} 2Al'_{Hf} + 3O_o + V_o^{\bullet\bullet} \quad (4)$$

where Al'_{Hf} is the substitution of Al^{3+} for Hf^{4+} site.

On the other hand, according to the oxygen-ion drift model the sufficient amount of oxygen and its storage are needed prior to stable switching behavior.[32] Moreover, when V_{form} is applied, the so-called soft breakdown (SB) occurs and the initial oxide film resistance cannot be fully recovered.[1] Considering these, we can imply that the HRS degradation of Al_2O_3-based device during the switching is due to insufficiency of oxygen O^{-2} moveable species at the Ti/oxide interface which causes the accumulation of additional undesirable/unrecoverable oxygen vacancies V_o^{2+} during the RS process, leading to fast hard breakdown and device failure. On the other hand, no such of HRS degradation was observed for HfO_2-based device. The sufficient storage of movable oxygen O^{-2} is formed at the Ti/oxide interface and supplies reliable switching till the end, but the favorable oxygen gettering in case of HfO_2-based

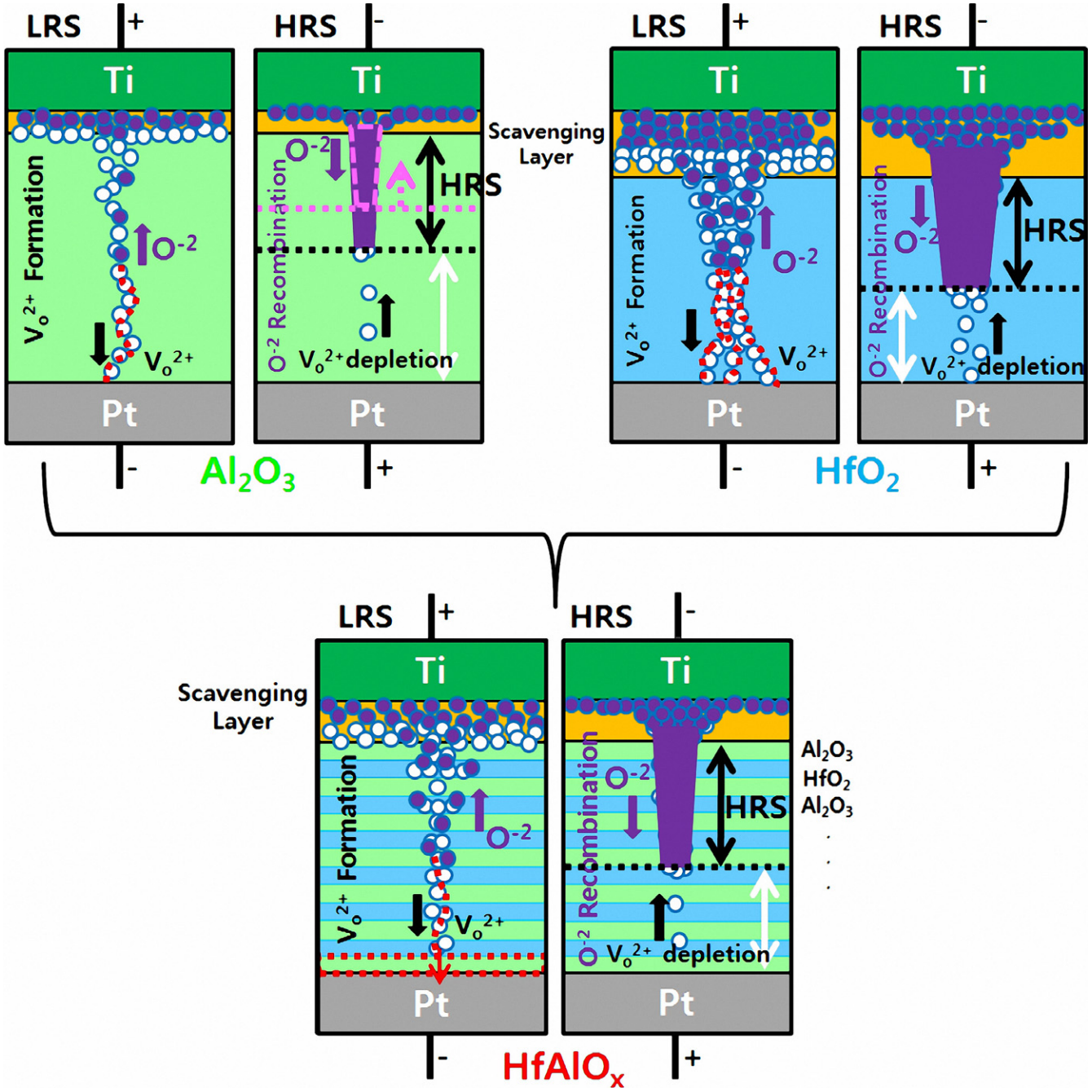

FIGURE 5 Proposed switching mechanism during the SET-RESET process for Al_2O_3, HfO_2 and $HfAlO_x$-based devices [Color figure can be viewed at wileyonlinelibrary.com]

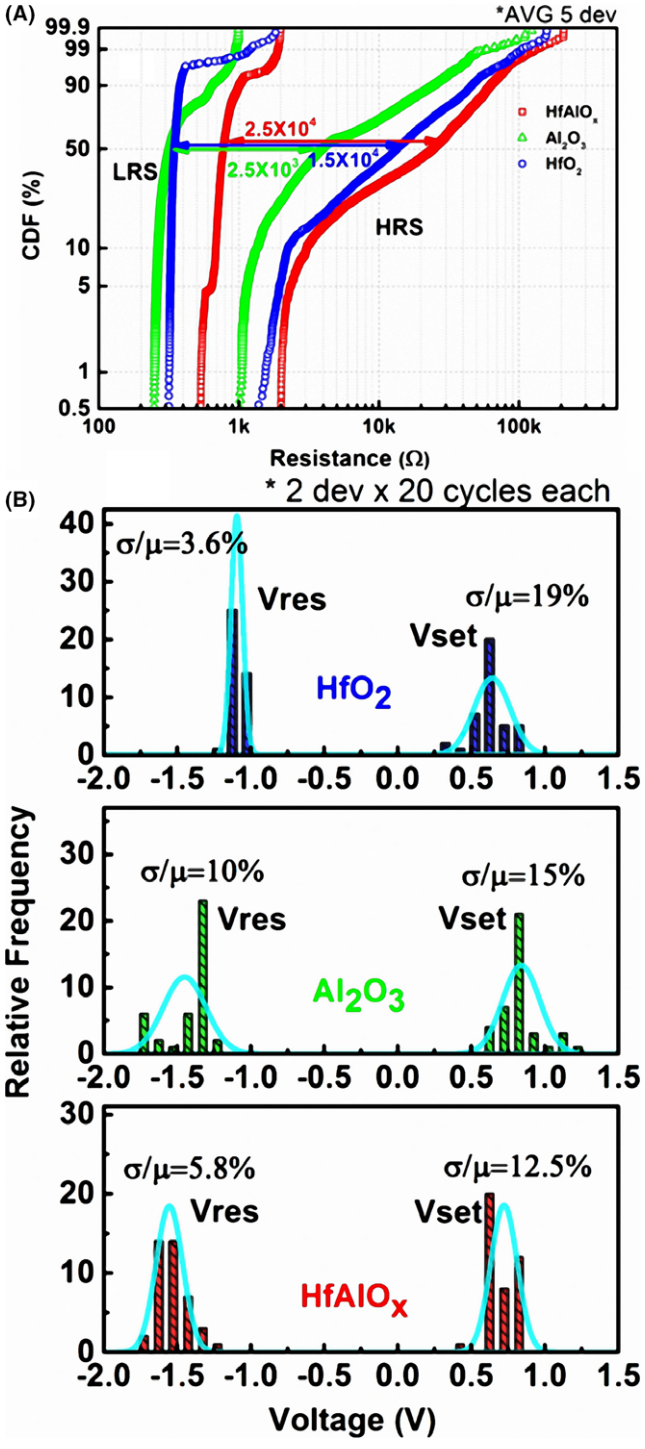

FIGURE 6 (A) Average distribution curves of the R_{OFF} and R_{ON} resistances for each device during all 400th dc sweeps and (B) the V_{SET} and V_{RES} statistics along the 400 dc sweeps for each device type, where σ is mean square error and μ is mean value [Color figure can be viewed at wileyonlinelibrary.com]

device causes the increase in filament shape leading to the more stochastic switching behavior and high current during RS cycling. To avoid these problems, stacking Al_2O_3 and HfO_2 thin films to form nanolaminated $HfAlO_x$ thin films benefits towards the better switching behavior in terms of reliable, uniform and low current RS process. In this case, the sufficiency of oxygen O^{-2} storage due to HfO_2 layers and thinning filament due to additional Al_2O_3 layers results in the higher reliability and uniformity of the RS behavior. No significant HRS degradation is observed during the whole course of cycling and LRS improvement is attributed to the large numbers of Al_2O_3 layers which causes thinning of the filament shape from Ti (TE) up to the Pt bottom electrode (BE) resulting in the filament higher resistivity and hence lower current SET-RESET processes.

Figure 6A shows the HRS and LRS variability along the full cycling period of each Al_2O_3, HfO_2 and $HfAlO_x$-based devices. The LRS average value in case of Al_2O_3 and HfO_2-based devices significantly deviate from that for $HfAlO_x$-based device, R_{LRS}=300 Ω and R_{LRS}=850 Ω, respectively. The higher resistance average value (25 kΩ) in HRS of $HfAlO_x$-based device is observed in comparison to Al_2O_3 (15 kΩ) and HfO_2 (4 kΩ)-based one. The effect of Hf–Al–O bond shrinkage due to Al(%) incorporation and consequent improvement of retention at LRS under 200°C of $HfAlO_x$ thin films, indicating its amorphous thermal stability, were recently reported.[33] The enhancement of LRS in our $HfAlO_x$-based device arises from "moderate" ΔG Gibbs free energy oxide formation of $HfAlO_x$ thin films, which influence scavenging effect at Ti/$HfAlO_x$ interface, i.e. shrinkage of filament shape with increasing amount of Al_2O_3 dopant. Additionally, since the SET-RESET switching partially relies on the thermal counterpart (Joule heat) to trigger the filament, enhanced amorphous thermal stability of $HfAlO_x$ thin films could play a vital role of keeping LRS at low resistance values during whole device operation time. It is been noted that with the scaling down of device, the deepest HRS state was observed for Al_2O_3-based device which confirms its high resistance ability.[34] Therefore, we suggest here that incorporation of thin Al_2O_3 oxide layers in the $HfAlO_x$-based device is responsible for deepest resistance in HRS of $HfAlO_x$ in comparison to the Al_2O_3 and HfO_2-based devices. In Figure 6B, the V_{SET} and V_{RESET} statistics are presented for each particular device type during 400 DC sweeps. To itself binary Al_2O_3, HfO_2-based devices show wide V_{SET} distribution. In HfO_2 material case, it is due to thick filament shape formation and as the result more stochastic V_{SET} behavior is observed. For Al_2O_3 material case, the insufficiency of movable oxygen O^{-2} species degrades the HRS and leads to consecutive shift of the V_{SET} behavior towards the higher voltages. However, improved balance in between V_{SET} and V_{RESET} statistics can be achieved in case of intermixing Al_2O_3 and HfO_2 thin films to form the $HfAlO_x$ nanolaminate. It can be noticed that the $HfAlO_x$-based device shows enhanced uniformity trade-off of V_{SET} and V_{RESET} distributions in between to just Al_2O_3 and HfO_2-based devices.

Figure 7A,B demonstrates *I–V* self-compliance switching curves of each Al_2O_3, HfO_2 and $HfAlO_x$-based device during the first 100 and last 400 cycles, respectively. The significant current reduction can be observed in case of $HfAlO_x$-based device compared with Al_2O_3 and HfO_2-based ones. The average current values I_{SET} and I_{RES} of $HfAlO_x$-based device are 1.7 mA and −1.7 mA, respectively. At the same time the average current values for Al_2O_3 and HfO_2-based device equals more than 3.2 mA. The total trend of slight current increase in comparison of first and last RS cycles can be noticed for all devices. In addition, the lowest V_{SET}-V_{RESET} voltages are found in case of HfO_2-based device, whereas for Al_2O_3 and $HfAlO_x$-based devices it is a little bit higher (±0.23 V). Particularly, the higher V_{SET}-V_{RESET} voltages of $HfAlO_x$-based device is believed due to Al_2O_3 thin layers incorporation since the V_{SET}-V_{RESET} voltages have the same average value as for Al_2O_3-based device.

Figure 8 shows the scattered distribution plots of RS dynamics during the SET-RESET processes of Al_2O_3, HfO_2 and $HfAlO_x$-based devices. Lower current and power distributions during the SET process are observed for $HfAlO_x$-based device, while these distributions for Al_2O_3 and HfO_2-based one show much higher average values of current and power as shown in Figure 8A. In addition, current distribution can be roughly fitted with the linear function of $y = a + b \cdot x$ while power distribution tends to be fitted within allometric function of $y = a \cdot x^b$. On the other hand, lower current and power distributions during the RESET

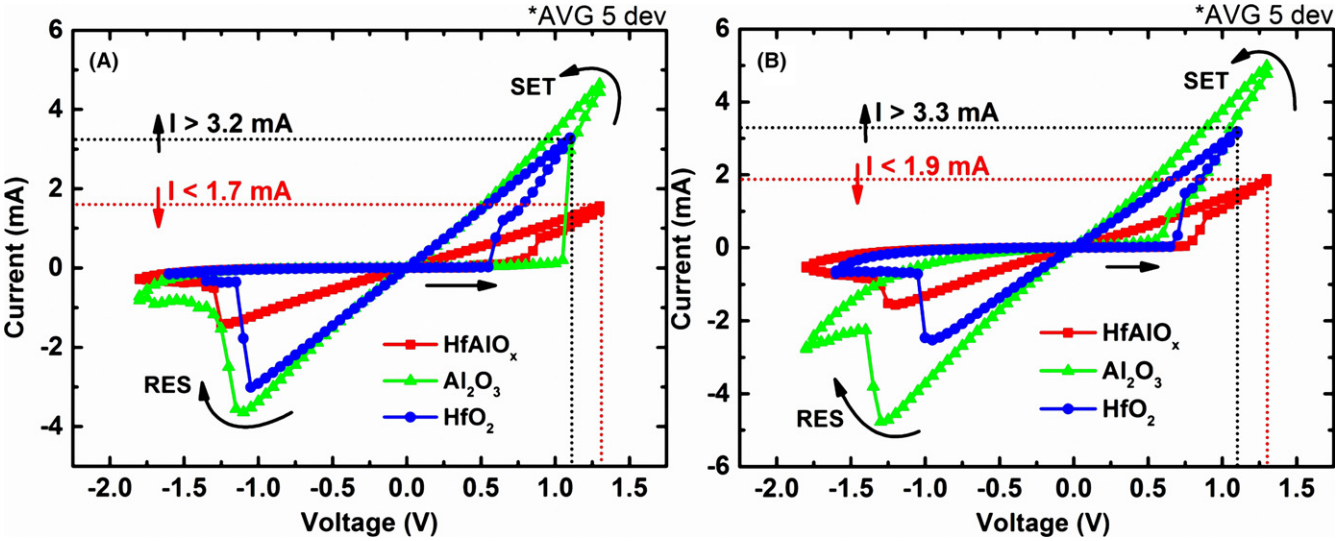

FIGURE 7 The *I–V* self-compliance characteristics curves for each Al_2O_3, HfO_2 and $HfAlO_x$-based device. The average RS switching curves of each device during the first 100th cycles (A) and during the last 400th cycles (B) [Color figure can be viewed at wileyonlinelibrary.com]

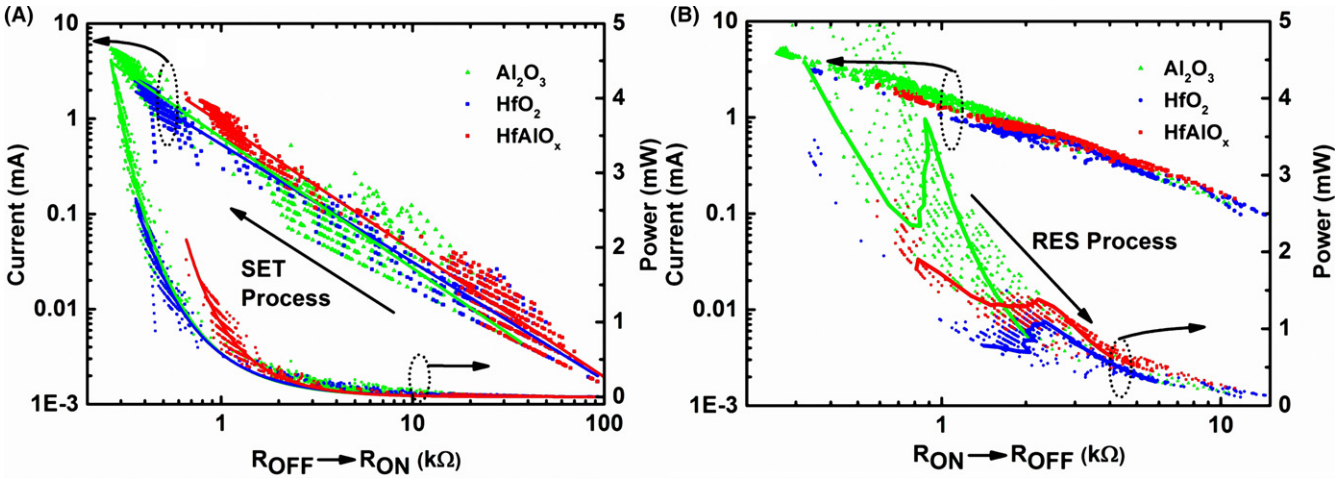

FIGURE 8 The scattered plot distributions along all cycles in terms of resistance vs current and power during the SET (A) and RESET (B) processes, respectively, for each Al_2O_3, HfO_2 and $HfAlO_x$-based device [Color figure can be viewed at wileyonlinelibrary.com]

process were observed for the HfO_2-based device in comparison to Al_2O_3 and $HfAlO_x$-based one in Figure 8B. The bold line curves represent the similar families' curves of power needed for each device during the cycling. Interestingly, the power "barrier" like behavior is observed for each device during the RS process. We believe that it is attributed to the oxide material properties itself and dissolution of the filament cone(tip) at the bottom electrode is appearing to be highly energy consuming process. Particularly, Al_2O_3-based device showed the biggest power "barrier" average value, which is also one of the reasons of its RESET failure during the RS process and as a result consecutive increase in resistance in HRS occurs. However, much lower power "barrier" average values during the RESET process were observed for HfO_2 and $HfAlO_x$-based devices. Moreover, slight increase in such power "barrier" in case of $HfAlO_x$-based device can be attributed to the multiple Al_2O_3 thin layers incorporation.

Figure 9A-C compares the endurance characteristics of $HfAlO_x$, HfO_2 and Al_2O_3-based devices, respectively. The good endurance characteristics of up to 10^5 cycles are obtained in case of $HfAlO_x$-based devices while Al_2O_3-based and HfO_2-based one show endurance up to 10^4 cycles only. The high variability in HRS & LRS during AC switching in case of HfO_2-based device and fast HRS degradation of Al_2O_3-based devices can be explicitly seen as well. As described above, this is due to their material properties itself and as was described above specific behavior at Ti/oxide interface in each case. In Figure 9D the excellent retention characteristics of up to 7×10^3 seconds are shown for each device. Although the read voltage V_{READ}=0.5 V is quite high, no significant degradation was observed during the whole stressing time.

4 | CONCLUSION

The uniform and higher self-compliance resistive switching behaviors with HRS (~25 kΩ at −1.8V) & LRS (~750 Ω at 1.3 V) are obtained in case of Ti/$HfAlO_x$/Pt ReRAM devices during the whole 400 DC cycling process. The high R_{OFF}/R_{ON} ratio (>10^2) and endurance up to (>10^5)

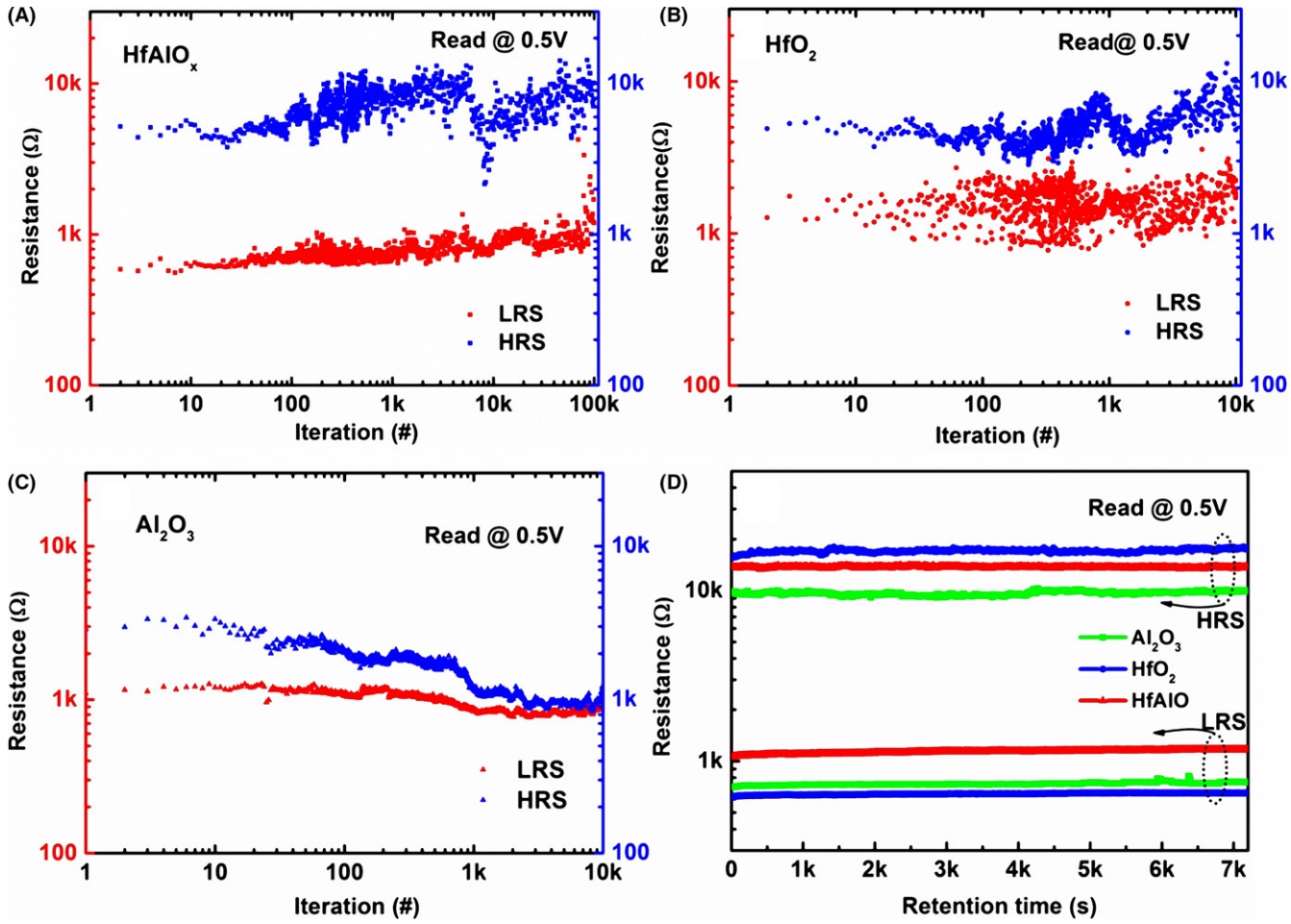

FIGURE 9 The endurance characteristics of $HfAlO_x$ (A), HfO_2 (B) and Al_2O_3 (C) devices, respectively. The retention characteristics under 0.5/−0.5 V read voltages during 2 hours for all devices are compared in (D) [Color figure can be viewed at wileyonlinelibrary.com]

cycles are consistent during the whole DC and AC RS performance. Such an improvement is attributed to the Al_2O_3 incorporated layers' confinement property of the RS filament in $HfAlO_x$ thin films. The higher oxygen content at the Ti/oxide interface is found for $HfAlO_x$ thin films, which is considered as an efficient oxygen storage leading to more reliable resistance switching process. From power "barrier"-like behavior aforementioned, $HfAlO_x$-based device is found to be at most working in low power at the SET process, while HfO_2-based device at the RESET process. Further, compared to HfO_2, more amorphous $HfAlO_x$ phase is observed, correlating with more densely packed and comparative stronger bonding of Hf-Al-O thin films within intermixed Al_2O_3/HfO_2 multiple oxide layers. Our finding indicates that Al incorporation into ALD $HfAlO_x$ thin films could be efficient way to improve resistive switching behavior compared to just binary ALD Al_2O_3 and HfO_2 thin films.

ACKNOWLEDGMENTS

This research was supported by Basic Science Research Program through National Research Foundation of Korea (NRF) funded by the Ministry of Education, Science and Technology (NRF-2015R1D1A1A01060300).

REFERENCES

1. Wong H-SP, Lee H-Y, Yu S, et al. Metal–oxide RRAM. *Proc IEEE*. 2012;100:1951-1970.
2. Prakash A, Jana D, Maikap S, et al. TaO_x-based resistive switching memories: prospective and challenges. *Nanoscale Res Lett*. 2013;8:1-17.
3. Tsunoda K, Kinoshita K, Noshiro H, et al. 2007. Low power and high speed switching of Ti-doped NiO ReRAM under the unipolar voltage source of less than 3 V. IEEE International Electron Devices Meeting (IEDM), Washington, DC, USA, 767-770.
4. Jeong HY, Lee JY, Choi SY, et al. Interface-engineered amorphous TiO_2-based resistive memory devices. *Adv Func Mater*. 2010;20:3912-3917.
5. Lin C-Y, Wu C-Y, Wu C-Y, et al. Effect of top electrode material on resistive switching properties of film memory devices. *IEEE Electron Device Lett*. 2007;28:366-368.
6. Ueki M, Akeuchi K, Yamamoto T, et al. 2015. Low-power embedded ReRAM technology for IoT applications. IEEE Symposium on (VLSI) Circuits, Kyoto, Japan. T108-T109.
7. Prakash A, Park J, Song J, et al. Demonstration of low power 3-bit multilevel cell characteristics in a TaO_x-based RRAM by stack engineering. *IEEE Electron Device Lett*. 2015;36:32-34.
8. Lee H-Y, Chen P-S, Wang C-C, et al. Low-power switching of nonvolatile resistive memory using hafnium oxide. *Jpn J Appl Phys*. 2007;46:2175-2179.
9. Lee H, Chen Y, Chen P, et al. Low-power and nanosecond switching in robust hafnium oxide resistive memory with a thin Ti cap. *IEEE Electron Device Lett*. 2010;31:44-46.
10. Lee H, Chen P, Wu T, et al. 2008. Low power and high speed bipolar switching with a thin reactive Ti buffer layer in robust HfO_2 based RRAM. IEEE International Electron Devices Meeting (IEDM). San Francisco, CA, USA. 1-4.
11. Kim CH, Ahn Y, Son JY, et al. $SrTiO_3$-based resistive switching memory device with graphene nanoribbon electrodes. *J Am Ceram Soc*. 2016;99:9-11.
12. Ho YD, Chen KR, Huang CL, et al. Resistive switching behaviors of sol-gel-derived $MgNb_2O_6$ thin films on ITO/glass substrate. *J Am Ceram Soc*. 2014;97:3544-3548.
13. Benoist A, Blonkowski S, Jeannot S, et al. 2014. 28 nm Advanced CMOS resistive RAM solution as embedded non-volatile memory. IEEE International Reliability Physics Symposium (IRPS), Waikoloa, HI, USA. 2E.6.1-2E.6.5.
14. Fantini A, Goux L, Degraeve R, et al. 2013. Intrinsic switching variability in HfO_2 RRAM. 5th IEEE International Memory Workshop (IMW), Monterey, CA, USA. 30-33.
15. Prakash A, Deleruyelle D, Song J, et al. Resistance controllability and variability improvement in a TaO_x-based resistive memory for multilevel storage application. *Appl Phys Lett*. 2015;106:2331041-2331044.
16. Young-Fisher KG, Bersuker G, Butcher B, et al. Leakage current-forming voltage relation and oxygen gettering in HfO_x RRAM devices. *IEEE Electron Device Lett*. 2013;34:750-752.
17. Calka P, Sowinska M, Bertaud T, et al. Engineering of the chemical reactivity of the Ti/HfO_2 interface for RRAM: experiment and theory. *ACS Appl Mater Interfaces*. 2014;6:5056-5060.
18. Bersuker G, Yum J, Vandelli L, et al. Grain boundary-driven leakage path formation in HfO_2 dielectrics. *Solid-State Electron*. 2011;65:146-150.
19. Park PK, Kang S-W. Enhancement of dielectric constant in HfO_2 thin films by the addition of Al_2O_3. *Appl Phys Lett*. 2006;89:1929051-1929053.
20. Wang T, Ekerdt JG, et al. Structure versus thermal stability: the periodic structure of atomic layer deposition-grown Al-incorporated HfO_2 films and its effects on amorphous stabilization. *Chem Mater*. 2011;23:1679-1685.
21. Bersuker G, Gilmer D, Veksler D, et al. Metal oxide resistive memory switching mechanism based on conductive filament properties. *J Appl Phys*. 2011;110:1245181-12451812.
22. Calka P, Martinez E, Delaye V, et al. Chemical and structural properties of conducting nanofilaments in TiN/HfO_2-based resistive switching structures. *Nanotechnology*. 2013;24:0857061-0857069.
23. Lanza M, Zhang K, Porti M, et al. Grain boundaries as preferential sites for resistive switching in the HfO_2 resistive random access memory structures. *Appl Phys Lett*. 2012;100:1235081-1235084.
24. Padovani A, Larcher L, Pirrotta O, et al. Microscopic modeling of HfO_x RRAM operations: from forming to switching. *IEEE Trans Electron Devices*. 2015;62:1998-2006.
25. McPherson JW, Kim J, Shanware A, et al. Trends in the ultimate breakdown strength of high dielectric-constant materials. *IEEE Trans Electron Devices*. 2003;50:1771-1778.
26. Park PK, Cha E-S, Kang S-W, et al. Interface effect on dielectric constant of HfO_2/Al_2O_3 nanolaminate films deposited by plasma-enhanced atomic layer deposition. *Appl Phys Lett*. 2007;90:2329061-2329063.
27. Fantini A, Goux L, Clima S, et al. 2014. Engineering of $Hf_{1-x}Al_xO_y$ amorphous dielectrics for high-performance RRAM

applications. IEEE 6th International Memory Workshop (IMW), Taipei, Taiwan. 1-4.
28. Lee M-J, Lee CB, Lee D, et al. A fast, high-endurance and scalable non-volatile memory device made from asymmetric Ta_2O_{5-x}/TaO_{2-x} bilayer structures. *Nat Mater*. 2011;10:625-630.
29. Yang J-B, Chang T-C, Huang J-J, et al. Influence of oxygen concentration on self-compliance RRAM in indium oxide film. *IEEE Electron Device Lett*. 2014;35:909-911.
30. Dean JA, Lange NA, eds. 1985. Lange's handbook of chemistry. 15th ed. *Section 6 thermodynamic properties*. McGraw Hill Book Co., New York, NY. 1561p.
31. Kröger F, Vink H. Relations between the concentrations of imperfections in crystalline solids. *Solid State Phys*. 1956;3:307-435.
32. Chen B, Kang JF, Gao B, et al. Endurance degradation in metal oxide-based resistive memory induced by oxygen ion loss effect. *IEEE Electron Device Lett*. 2013;34:1292-1294.
33. Traoré B, Blaise P, Vianello E, et al. On the origin of low-resistance state retention failure in HfO_2-based RRAM and impact of doping/alloying. *IEEE Trans Electron Devices*. 2015;62:4029-4036.
34. Goux L, Fantini A, Degraeve R. et al. 2013. Understanding of the intrinsic characteristics and memory trade-offs of sub-μA filamentary RRAM operation. IEEE Symposium on VLSI Technology (VLSIT), Kyoto, Japan. T162-T163.

How to cite this article: Sokolov AS, Son SK, Lim D, et al. Comparative study of Al_2O_3, HfO_2, and $HfAlO_x$ for improved self-compliance bipolar resistive switching. *J Am Ceram Soc*. 2017;100:5638–5648. https://doi.org/10.1111/jace.15100